

# Homologous Series of 2D Chalcogenides $\text{Cs}-\text{Ag}-\text{Bi}-\text{Q}$ ( $\text{Q} = \text{S, Se}$ ) with Ion-Exchange Properties

Jing Zhao,<sup>†,‡,§,ID</sup> Saiful M. Islam,<sup>‡</sup> Shiqiang Hao,<sup>§</sup> Gangjian Tan,<sup>‡,ID</sup> Constantinos C. Stoumpos,<sup>‡,ID</sup> Chris Wolverton,<sup>§,ID</sup> Haijie Chen,<sup>‡,ID</sup> Zhongzhen Luo,<sup>‡</sup> Rukang Li,<sup>†</sup> and Mercouri G. Kanatzidis\*,<sup>‡,ID</sup>

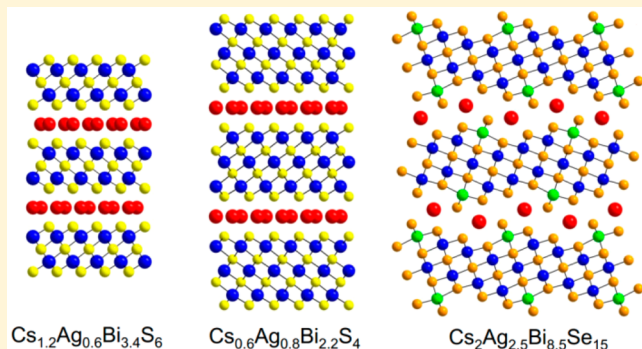
<sup>†</sup> Beijing Center for Crystal Research and Development, Technical Institute of Physics and Chemistry, Chinese Academy of Sciences, Beijing 100190, P. R. China

<sup>‡</sup> Department of Chemistry, Northwestern University, Evanston, Illinois 60208, United States

<sup>§</sup> Department of Materials Science and Engineering, Northwestern University, Evanston, Illinois 60208, United States

## S Supporting Information

**ABSTRACT:** Four new layered chalcogenides  $\text{Cs}_{1.2}\text{Ag}_{0.6}\text{Bi}_{3.4}\text{S}_6$ ,  $\text{Cs}_{1.2}\text{Ag}_{0.6}\text{Bi}_{3.4}\text{Se}_6$ ,  $\text{Cs}_{0.6}\text{Ag}_{0.8}\text{Bi}_{2.2}\text{S}_4$ , and  $\text{Cs}_2\text{Ag}_{2.5}\text{Bi}_{8.5}\text{Se}_{15}$  are described.  $\text{Cs}_{1.2}\text{Ag}_{0.6}\text{Bi}_{3.4}\text{S}_6$  and  $\text{Cs}_{1.2}\text{Ag}_{0.6}\text{Bi}_{3.4}\text{Se}_6$  are isostructural and have a hexagonal  $P6_3/mmc$  space group; their structures consist of  $[\text{Ag}/\text{Bi}]_2\text{Q}_3$  ( $\text{Q} = \text{S, Se}$ ) quintuple layers intercalated with disordered Cs cations.  $\text{Cs}_{0.6}\text{Ag}_{0.8}\text{Bi}_{2.2}\text{S}_4$  also adopts a structure with the hexagonal  $P6_3/mmc$  space group and its structure has an  $[\text{Ag}/\text{Bi}]_3\text{S}_4$  layer intercalated with a Cs layer.  $\text{Cs}_{1.2}\text{Ag}_{0.6}\text{Bi}_{3.4}\text{S}_6$  and  $\text{Cs}_{0.6}\text{Ag}_{0.8}\text{Bi}_{2.2}\text{S}_4$  can be ascribed to a new homologous family  $\text{A}_x[\text{M}_m\text{S}_{1+m}]$  ( $m = 1, 2, 3, \dots$ ).  $\text{Cs}_2\text{Ag}_{2.5}\text{Bi}_{7.5}\text{Se}_{15}$  is orthorhombic with  $Pnmm$  space group, and it is a new member of the  $\text{A}_2[\text{M}_{5+n}\text{Se}_{9+n}]$  homology with  $n = 6$ . The Cs ions in  $\text{Cs}_{1.2}\text{Ag}_{0.6}\text{Bi}_{3.4}\text{S}_6$  and  $\text{Cs}_{0.6}\text{Ag}_{0.8}\text{Bi}_{2.2}\text{S}_4$  can be exchanged with other cations, such as  $\text{Ag}^+$ ,  $\text{Cd}^{2+}$ ,  $\text{Co}^{2+}$ ,  $\text{Pb}^{2+}$ , and  $\text{Zn}^{2+}$  forming new phases with tunable band gaps between 0.66 and 1.20 eV.  $\text{Cs}_{1.2}\text{Ag}_{0.6}\text{Bi}_{3.4}\text{S}_6$  and  $\text{Cs}_{0.6}\text{Ag}_{0.8}\text{Bi}_{2.2}\text{S}_4$  possess extremely low thermal conductivity ( $<0.6 \text{ W}\cdot\text{m}^{-1}\cdot\text{K}^{-1}$ ).



## INTRODUCTION

A layered structure is one where intralayer bonding is more significant than interlayer bonding. When anionic covalent frameworks are charge balanced by alkali metal ions,<sup>1–3</sup> the presence of alkali metals force the covalent frameworks to form around them. Thus, alkali metal chalcogenides tend to form chain, layered, or tunneled structures depending on the  $\text{A}_2\text{Q}/\text{MQ}$  ratios ( $\text{Q} = \text{S, Se, Te}$ ).<sup>4</sup> The highly anisotropic nature of the materials may lead to the possibilities of tailoring the band gaps<sup>5,6</sup> and can give rise to attractive and unusual physical properties that makes them outstanding for applications in the fields of topological quantum science,<sup>7–13</sup> thermoelectricity,<sup>14–16</sup>  $\gamma$ -ray detection,<sup>17,18</sup> second-harmonic generation,<sup>19</sup> optical data storage,<sup>20</sup> superconductivity,<sup>21,22</sup> charge density wave formation, and photovoltaics.<sup>23,24</sup>

Bismuth chalcogenide compounds are a special class because they exhibit amazingly diverse compositions and structures.<sup>25,26</sup> The trivalent Bi atoms in the structures can have coordination numbers varying from 3 to 9, and the inert  $6s^2$  lone pair of electrons defines the electronic character of the compounds. In these compounds the  $\text{BiQ}_6$  ( $\text{Q} = \text{S, Se, Te}$ ) octahedra can combine by edge or face sharing to form blocks or modules that are fragments excised from the  $\text{NaCl}$ -,  $\text{Bi}_2\text{Te}_3$ -,  $\text{CdI}_2$ -, and  $\text{Sb}_2\text{Se}_3$ -type structures.<sup>4,25,27,28</sup> Furthermore, Bi atoms can share sites with similar sized cations, such as alkali or alkaline earth

metals,  $\text{Cu}^+$ ,  $\text{Pb}^{2+}$ ,  $\text{Sn}^{2+}$ ,  $\text{Ag}^+$ ,  $\text{Cd}^{2+}$  or lanthanides.<sup>29–32</sup> Ternary or quaternary alkali metal chalcogenides  $\text{A}/\text{M}/\text{Bi}/\text{Q}$  ( $\text{A} = \text{Li, K, Rb, Cs}; \text{M} = \text{Sn, Pb, Ag, Cd}; \text{Q} = \text{S, Se, Te}$ )<sup>28</sup> form readily and tend to possess tunneled or layered structures. For example, the  $\text{A}_m[\text{M}_{1+l}\text{Se}_{2+l}]_{2m}[\text{M}_{1+2l+n}\text{Se}_{3+3l+n}]$  ( $\text{A} = \text{alkali metal, M} = \text{Sn and Bi}$ ) homologous superseries<sup>33,34,29</sup> features compounds with tunneled structures, while the members of the  $\text{Cs}_4[\text{Bi}_{2n+4}\text{Te}_{3n+6}]$ ,<sup>4</sup>  $\text{CsM}_m\text{Bi}_3\text{Te}_{5+m}$ ,<sup>35,36</sup>  $[\text{MTe}]_n[\text{Bi}_2\text{Te}_3]_m$  ( $\text{M} = \text{Ge, Sn, Pb}$ ),<sup>37–45</sup> and  $\text{A}_2[\text{M}_{5+n}\text{Se}_{9+n}]$  ( $\text{A} = \text{Rb, Cs}; \text{M} = \text{Bi, Ag, Cd}$ )<sup>30</sup> series possess layered structures. Recently, we reported the family  $\text{A}_x\text{Cd}_x\text{Bi}_{4-x}\text{Q}_6$  ( $\text{A} = \text{Cs, Rb, K}; \text{Q} = \text{S and A} = \text{Cs}; \text{Q} = \text{Se}$ )<sup>46</sup> of new compounds which also possess a layered structure.

The discovery and classification of homologous series make structure design and prediction possible and they are part of a growing toolbox for the creation of new materials.<sup>26,47,48</sup> Herein, we present the synthesis, structure and characterization of four new compounds  $\text{Cs}_{1.2}\text{Ag}_{0.6}\text{Bi}_{3.4}\text{S}_6$ ,  $\text{Cs}_{1.2}\text{Ag}_{0.6}\text{Bi}_{3.4}\text{Se}_6$ ,  $\text{Cs}_{0.6}\text{Ag}_{0.8}\text{Bi}_{2.2}\text{S}_4$ , and  $\text{Cs}_2\text{Ag}_{2.5}\text{Bi}_{8.5}\text{Se}_{15}$ . They crystallize in three different structure types. All compounds have layered structures with intercalated  $\text{Cs}^+$  cations. We show that Cs cations reside between the layers of  $\text{Cs}_{1.2}\text{Ag}_{0.6}\text{Bi}_{3.4}\text{S}_6$  and  $\text{Cs}_{0.6}\text{Ag}_{0.8}\text{Bi}_{2.2}\text{S}_4$  and can be ion-exchanged with other cations without structural

Received: June 19, 2017

Published: August 15, 2017

change of the frameworks (topotactically). Thus, they provide a “soft chemistry” route to generate new materials.<sup>46,49–51</sup>  $\text{Cs}_{1.2}\text{Ag}_{0.6}\text{Bi}_{3.4}\text{S}_6$  and  $\text{Cs}_{0.6}\text{Ag}_{0.8}\text{Bi}_{2.2}\text{S}_4$  are members of a new homologous family  $\text{A}_x[\text{M}_m\text{S}_{1+m}]$  ( $m = 1, 2, 3\dots$ ) while  $\text{Cs}_2\text{Ag}_{2.5}\text{Bi}_{7.5}\text{Se}_{15}$  is a new member of the  $\text{A}_2[\text{M}_{5+n}\text{Se}_{9+n}]$  homology with  $n = 6$ .

## EXPERIMENTAL SECTION

**Reagents.** All chemicals were used as-obtained, silver metal (99.99%, Sigma-Aldrich), bismuth metal (99.9%, Strem Chemicals), sulfur pellets (99.99%, Sigma-Aldrich), and selenium pellets (99.99%, Sigma-Aldrich).  $\text{AgNO}_3$  (ACS grade, Sigma-Aldrich),  $\text{CdCl}_2$  (ACS grade, Mallinckrodt Baker, Inc.),  $\text{Co}(\text{NO}_3)_2 \cdot 6\text{H}_2\text{O}$  (ACS grade, Mallinckrodt Baker, Inc.),  $\text{ZnCl}_2$  (ACS grade, Columbus Chemical Industries, Inc.), and  $\text{Pb}(\text{NO}_3)_2$  (ACS grade, Columbus Chemical Industries, Inc.).  $\text{Cs}_2\text{S}$  and  $\text{Cs}_2\text{Se}$  were synthesized by reacting stoichiometric amounts of the elements in liquid ammonia as described elsewhere.<sup>52</sup>

**Synthesis.**  $\text{Cs}_{1.2}\text{Ag}_{0.6}\text{Bi}_{3.4}\text{S}_6$ . Single crystals of  $\text{Cs}_{1.2}\text{Ag}_{0.6}\text{Bi}_{3.4}\text{S}_6$  were obtained by combining 0.0894 g  $\text{Cs}_2\text{S}$  (0.3 mmol), 0.0539 g Ag (0.5 mmol), 0.3030 g Bi (1.45 mmol), and 0.0706 g S (2.2 mmol) together in a 9 mm carbon coated fused silica tube and it was flame-sealed at a vacuum of  $\sim 10^{-4}$  mbar. The tube was put into a programmable furnace and heated to 300 °C in 6 h, held at this temperature for 5 h for total melt of the sulfur, heated to 880 °C in 7 h, and held at 880 °C for 72 h, cooled to 450 °C in 96 h, and held at this temperature for 1 h followed by cooling to RT in 2 h. Black plate-like crystals with the longest edge up to 0.1 mm were obtained. Pure phase (with no observable impurities from PXRD pattern) of  $\text{Cs}_{1.2}\text{Ag}_{0.6}\text{Bi}_{3.4}\text{S}_6$  can be obtained with the same starting ratio but with a faster cooling rate of cooling from 880 to 450 °C in 24 h.

$\text{Cs}_{1.2}\text{Ag}_{0.6}\text{Bi}_{3.4}\text{Se}_6$ . Single crystals of  $\text{Cs}_{1.2}\text{Ag}_{0.6}\text{Bi}_{3.4}\text{Se}_6$  were obtained by the same starting molar ratio of  $\text{Cs}_{1.2}\text{Ag}_{0.6}\text{Bi}_{3.4}\text{S}_6$  but changing sulfur to selenium by mixing 0.103 g  $\text{Cs}_2\text{Se}$  (0.3 mmol), 0.0539 g Ag (0.5 mmol), 0.3030 g Bi (1.45 mmol), and 0.1737 g Se (2.2 mmol) together in a 9 mm carbon coated fused silica tube and flame-sealed at  $\sim 10^{-4}$  mbar. Using the same heating profile as  $\text{Cs}_{1.2}\text{Ag}_{0.6}\text{Bi}_{3.4}\text{S}_6$ , this experiment yielded black plate-like crystals of  $\text{Cs}_{1.2}\text{Ag}_{0.6}\text{Bi}_{3.4}\text{Se}_6$  large enough for single crystal X-ray diffraction measurement. The phase purity of the obtained sample is  $\sim 90\%$ , Figure S1 of the Supporting Information (SI).

$\text{Cs}_{0.6}\text{Ag}_{0.8}\text{Bi}_{2.2}\text{S}_4$ .  $\text{Cs}_{0.6}\text{Ag}_{0.8}\text{Bi}_{2.2}\text{S}_4$  crystals were obtained using the starting materials of 0.0745 g  $\text{Cs}_2\text{S}$  (0.25 mmol), 0.0539 g Ag (0.5 mmol), 0.209 g Bi (1 mmol), and 0.0722 g S (2.25 mmol). The mixture was loaded in a 9 mm carbon coated fused silica tube in a dry, nitrogen-filled glovebox. The tube was then placed in a programmable furnace and heated to 350 °C in 10 h and held at 350 °C for 6 h for the total melt of S, then heated to 750 °C in 12 h and soaked for 18 h, followed by slow cooling to 300 °C in 96 h and then held for 1 h, finally cooled to RT in 3 h. Black plate-like crystals were obtained. Pure phase of  $\text{Cs}_{0.6}\text{Ag}_{0.8}\text{Bi}_{2.2}\text{S}_4$  was obtained by combining 0.834 g  $\text{Cs}_2\text{S}$  (2.8 mmol), 0.0895 g Ag (0.83 mmol), 0.3521 g Bi (1.69 mmol), and 0.0926 g S (2.89 mmol) together in a carbon coated fused silica tube. The tube was heated to 350 °C in 6 h and held for 6 h, then heated to 750 °C in 12 h and soaked for 24 h, followed by slow cooling to 300 °C in 32 h and then held for 1 h, and finally cooled to RT in 2 h. The  $\text{Cs}_{0.6}\text{Ag}_{0.8}\text{Bi}_{2.2}\text{S}_4$  pure phase was obtained with no observable extra peaks from the PXRD pattern.

$\text{Cs}_2\text{Ag}_{2.5}\text{Bi}_{8.5}\text{Se}_{15}$ . Synthesis was conducted to obtain  $\text{Cs}_{0.6}\text{Ag}_{0.8}\text{Bi}_{2.2}\text{Se}_4$  crystals with the same starting molar ratio used to obtain  $\text{Cs}_{0.6}\text{Ag}_{0.8}\text{Bi}_{2.2}\text{S}_4$ . The starting materials are 0.0862 g  $\text{Cs}_2\text{Se}$  (2.8 mmol), 0.539 g Ag (0.83 mmol), 0.209 g Bi (1.69 mmol), and 0.1777 g Se (2.89 mmol). The starting materials were combined together in a 9 mm fused silica tube in a dry, nitrogen-filled glovebox. The tube was evacuated to  $\sim 10^{-4}$  mbar and flame-sealed. The tube was heated to 300 °C in 6 h, held for 6 h, and then heated to 750 °C in 12 h and held for 18 h, then cooled down to 300 °C in 96 h and held for 1 h followed by cooling to room temperature (RT) in 3 h. Bar-like crystals

were obtained for single crystal diffraction and the purity of the obtained phase is  $\sim 90\%$ , Figure S1.

Finally,  $\text{Cs}_2\text{Ag}_{2.5}\text{Bi}_{8.5}\text{Se}_{15}$  (with a nominal formula of  $\text{Cs}_{0.53}\text{Ag}_{0.67}\text{Bi}_{2.26}\text{Se}_4$ ) with  $Pnma$  space group instead of  $\text{Cs}_{0.6}\text{Ag}_{0.8}\text{Bi}_{2.2}\text{Se}_4$  ( $P6_3/mmc$  space group) was obtained. When trying to obtain better crystals of  $\text{Cs}_2\text{Ag}_{2.5}\text{Bi}_{8.5}\text{Se}_{15}$  with different starting material ratios, a reported compound  $\text{Cs}_2\text{Ag}_{1.8}\text{Bi}_{7.5}\text{Se}_{13}$ <sup>30</sup> was also obtained but the structure of this compound was rerefined and the CIF file is given in the SI.

**Powder X-ray Diffraction.** The purity of the samples was characterized by Rigaku Miniflex powder X-ray diffractometer with Ni-filtered  $\text{Cu K}\alpha$  radiation operating at 40 kV and 15 mA. The scanning width is 0.02° and a collecting rate of 10°/min was used. Simulated powder X-ray diffraction (PXRD) pattern was obtained by using the CIF file of the refined structure by using the Visualizer software package of the program FINDIT.

**Single Crystal X-ray Diffraction.** The single crystals used to conduct X-ray diffraction measurements were adhered to the tips of glass fibers with glue. STOE IPDS II single crystal diffractometer was operated at 50 kV and 40 mA with  $\text{Mo K}\alpha$  radiation ( $\lambda = 0.71073 \text{ \AA}$ ). Data collection were conducted by using X-Area software,<sup>53</sup> integration were operated in X-RED, and numerical absorption corrections were applied with X-SHAPE.<sup>53</sup> The crystal structures were solved via direct method and refined by SHELXTL program package.<sup>54</sup> Tables S1–S12 show the atomic coordinates and equivalent isotropic displacement parameters, anisotropic displacement parameters, and bond lengths of the title compounds.

**Scanning Electron Microscopy.** Quantitative microprobe analyses and crystal imaging of the compounds were performed using Hitachi S-3400 scanning electron microscope equipped with a PGT energy-dispersive X-ray analyzer. The data were acquired by an accelerating voltage of 25 kV, a probe current of 70 mA, and 60 s acquisition time. The compositions reported here are an average of a large number of independent measurements from given samples.

**Differential Thermal Analysis.** The ground single crystals of  $\text{Cs}_{1.2}\text{Ag}_{0.6}\text{Bi}_{3.4}\text{S}_6$  and  $\text{Cs}_{0.6}\text{Ag}_{0.8}\text{Bi}_{2.2}\text{S}_4$  with a mass about 40 mg were sealed in silica ampules under a vacuum of  $\sim 10^{-4}$  mbar. Differential Thermal Analysis (DTA) was performed with a computer-controlled Shimadzu DTA-50 thermal analyzer. A silica ampule containing alumina was placed on the reference side of the detector. The  $\text{Cs}_{1.2}\text{Ag}_{0.6}\text{Bi}_{3.4}\text{S}_6$  sample was heated to 750 °C and  $\text{Cs}_{0.6}\text{Ag}_{0.8}\text{Bi}_{2.2}\text{S}_4$  was heated to 620 °C at 10 °C/min followed by cooling at 10 °C/min to room temperature, and finally this cycle was repeated. The DTA products were examined with PXRD after the experiment.

**Ultraviolet–Visible Spectroscopy.** The ultraviolet–visible spectra were recorded, in the infrared region 500–2000 nm, with the use of UV-3600 Shimadzu UV-3600 PC double-beam, double-monochromator spectrophotometer. Finely ground samples were used to do the measurements at room temperature. By using the Kubelka–Munk equation absorption ( $\alpha/S$ ), data were obtained:  $\alpha/S = (1-R)^2/2R$ , where  $R$  is reflectance,  $\alpha$  is absorption coefficient, and  $S$  is scattering coefficient.<sup>55</sup> The fundamental absorption edge was obtained by linearly fitting the absorbance of the converted data.

**Ion-Exchange Experiments.** Ion-exchange experiments of  $\text{Cs}_{1.2}\text{Ag}_{0.6}\text{Bi}_{3.4}\text{S}_6$  and  $\text{Cs}_{0.6}\text{Ag}_{0.8}\text{Bi}_{2.2}\text{S}_4$  were conducted. The crystals of  $\text{Cs}_{1.2}\text{Ag}_{0.6}\text{Bi}_{3.4}\text{S}_6$  and  $\text{Cs}_{0.6}\text{Ag}_{0.8}\text{Bi}_{2.2}\text{S}_4$  ( $\sim 10.0 \text{ mg}$ ) were added into 0.2 mol/L water solution (10 mL) of  $\text{AgNO}_3$ ,  $\text{CdCl}_2$ ,  $\text{Co}(\text{NO}_3)_2 \cdot 6\text{H}_2\text{O}$ ,  $\text{ZnCl}_2$ , and  $\text{Pb}(\text{NO}_3)_2$ , respectively. The mixture kept shaking for 24 h at RT and was then isolated by filtration (through filter paper, Whatman no. 1); and washed several times with water and acetone then dried in air. Crystals after ion-exchange were hand-picked and analyzed with energy dispersive spectroscopy (EDS) analysis. The ground powder of  $\text{Cs}_{1.2}\text{Ag}_{0.6}\text{Bi}_{3.4}\text{S}_6$  and  $\text{Cs}_{0.6}\text{Ag}_{0.8}\text{Bi}_{2.2}\text{S}_4$  ( $\sim 100 \text{ mg}$ ) were added in 0.2 mol/L water solution (20 mL) of  $\text{AgNO}_3$ ,  $\text{CdCl}_2$ ,  $\text{Co}(\text{NO}_3)_2 \cdot 6\text{H}_2\text{O}$ ,  $\text{ZnCl}_2$ , and  $\text{Pb}(\text{NO}_3)_2$ , respectively. The mixture was kept under magnetic stirring for 24 h at RT. The solution was filtered and washed as previously mentioned and characterized with PXRD and UV–visible spectroscopy.

**Spark Plasma Sintering.** Phase pure samples of  $\text{Cs}_{1.2}\text{Ag}_{0.6}\text{Bi}_{3.4}\text{S}_6$  and  $\text{Cs}_{0.6}\text{Ag}_{0.8}\text{Bi}_{2.2}\text{S}_4$  were pulverized and hand ground into fine powders in a  $\text{N}_2$ -filled glovebox. The powders were then loaded into

graphite dies with a diameter of 10 mm for SPS at 763 K for 10 min under an axial pressure of 30 MPa. The relative mass density of the SPSed sample is about 97% for  $\text{Cs}_{1.2}\text{Ag}_{0.6}\text{Bi}_{3.4}\text{S}_6$  and 93% for  $\text{Cs}_{0.6}\text{Ag}_{0.8}\text{Bi}_{2.2}\text{S}_4$ .

**Thermal Conductivity.** The SPSed pellets were cut and polished into desired geometry with dimensions of  $\sim 6 \times 6 \times 2 \text{ mm}^3$  and coated with a thin layer of graphite to minimize the emissivity of the material. By using the laser flash diffusivity method in Netzsch LFA457 thermal diffusivity ( $D$ ) coefficients were measured perpendicular to the SPS pressure direction. The thermal diffusivity data were analyzed using a Cowan model with pulse correction. The total thermal conductivity was calculated from  $\kappa_{\text{tot}} = DC_p d$ , density ( $d$ ) is determined using the dimensions and mass of the SPSed sample. The specific heat capacity ( $C_p$ ) was estimated by the Dulong-Petit law  $C_p = 3R/\bar{M}$ , in which  $R$  is gas constant  $8.314 \text{ J mol}^{-1}\text{K}^{-1}$ , and  $\bar{M}$  is the average molar mass. The uncertainty of the thermal conductivity is estimated to be  $\sim 8\%$ .<sup>56</sup>

**Electrical Properties.** SPS-processed pellet were cut into bars ( $\sim 3 \times 3 \times 8 \text{ mm}^3$ ) perpendicular to the sintering pressure direction, and the samples were spray-coated with boron nitride to minimize outgassing, except where needed for electrical contact. The Seebeck coefficients and electrical conductivities were measured simultaneously on an Ulvac Riko ZEM-3 instrument under a low-pressure helium atmosphere. The uncertainty of the Seebeck coefficients and electrical conductivity measurements is  $\sim 5\%$ .<sup>56</sup>

**Density Functional Theory (DFT) Calculations.** The total energies and relaxed geometries were calculated by DFT using the exchange correlation functional within the generalized gradient approximation (GGA) of Perdew–Burke–Ernzerhof the exchange correlation functional with Projector Augmented Wave potentials.<sup>57</sup> We use periodic boundary conditions, a plane wave basis set, and Projector Augmented Wave potentials<sup>57</sup> as implemented in the Vienna ab initio simulation package.<sup>58</sup> The total energies were numerically converged to approximately 3 meV/cation using a basis set energy cutoff of 500 eV and dense  $k$ -meshes corresponding to 4000  $k$ -points per reciprocal atom in the Brillouin zone. Our theoretically relaxed  $\text{CsAgBi}_2\text{S}_4$  lattice constants for the  $P6_3/mmc$  crystal structure are  $a = 7.04 \text{ \AA}$ ,  $b = 4.09 \text{ \AA}$ , and  $c = 28.11 \text{ \AA}$ , which are in reasonable agreement with the experimentally measured lattice parameters,  $a = 4.0331(6) \text{ \AA}$ ,  $b = 4.0331(6) \text{ \AA}$ ,  $c = 30.438(6) \text{ \AA}$ . Building a small-unit-cell periodic atomic structure to represent  $\text{Cs}_{0.6}\text{Ag}_{0.8}\text{Bi}_{2.2}\text{S}_4$  is difficult, since Cs sites are partially occupied and certain Bi atoms occupy the Ag site. We thus used a simplified  $\text{CsAgBi}_2\text{S}_4$  stoichiometry, with no partially occupied Wyckoff sites as a model to simplify the problem.

**Phonon Dispersion Calculations.** To quantitatively explore the origin of lattice thermal conductivity at the atomic level, we utilize the Debye–Callaway model to quantitatively evaluate the value of lattice thermal conductivity of  $\text{CsAgBi}_2\text{S}_4$ . It is known that the Grüneisen parameters, which characterize the relationship between phonon frequency and crystal volume change, serve as a useful measure of the lattice anharmonicity and thus helpful to interpret the physical nature of lattice thermal conductivity behavior.<sup>59,60</sup> The phonon and Grüneisen dispersions are calculated using first-principles DFT phonon calculations within the quasi-harmonic approximation. The  $\text{CsAgBi}_2\text{S}_4$  phonon dispersions are calculated on a 128 atom cell at two volumes, one is the equilibrium volume  $V_0$ , and an isotropically compressed volume  $0.98V_0$ . Details of Grüneisen parameter calculations are given in the SI.

## RESULTS AND DISCUSSION

**Synthesis and Thermal Stability.** Single crystals of  $\text{Cs}_{1.2}\text{Ag}_{0.6}\text{Bi}_{3.4}\text{S}_6$ ,  $\text{Cs}_{1.2}\text{Ag}_{0.6}\text{Bi}_{3.4}\text{Se}_6$ ,  $\text{Cs}_{0.6}\text{Ag}_{0.8}\text{Bi}_{2.2}\text{S}_4$ , and  $\text{Cs}_2\text{Ag}_{2.5}\text{Bi}_{8.5}\text{Se}_{15}$  were obtained with a relatively slow cooling rate ( $\sim 5 \text{ }^\circ\text{C}/\text{h}$ ). Pure phases of  $\text{Cs}_{1.2}\text{Ag}_{0.6}\text{Bi}_{3.4}\text{S}_6$  and  $\text{Cs}_{0.6}\text{Ag}_{0.8}\text{Bi}_{2.2}\text{S}_4$  can be obtained by heating a mixture of  $\text{Cs}_2\text{S}$ , Ag, Bi, and S in sealed fused silica tubes at  $750 \text{ }^\circ\text{C}$  as indicated by the powder X-ray diffraction (PXRD) patterns, Figure 1(a). All compounds are black and stable in air, water, and acetone.

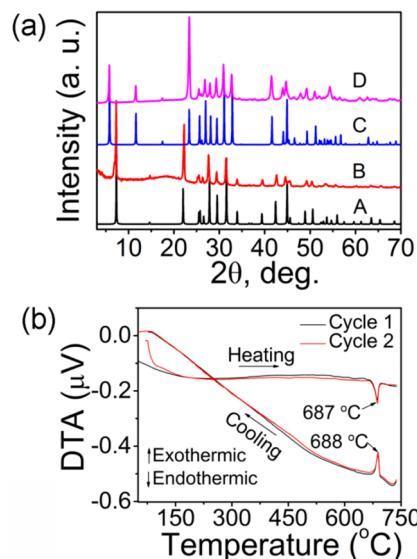


**Figure 1.** (a) Comparison of powder X-ray diffraction spectrum between synthesized and the simulated ones. A:  $\text{Cs}_{1.2}\text{Ag}_{0.6}\text{Bi}_{3.4}\text{S}_6$  simulated, B:  $\text{Cs}_{1.2}\text{Ag}_{0.6}\text{Bi}_{3.4}\text{S}_6$  synthesized, C:  $\text{Cs}_{0.6}\text{Ag}_{0.8}\text{Bi}_{2.2}\text{S}_4$  simulated, and D:  $\text{Cs}_{0.6}\text{Ag}_{0.8}\text{Bi}_{2.2}\text{S}_4$  synthesized. (b) The DTA curves of  $\text{Cs}_{0.94}\text{Ag}_{0.56}\text{Bi}_{2.24}\text{S}_4$ .

Energy-dispersive X-ray spectroscopy (EDS) was performed as semiquantitative elemental analysis of Cs, Ag, Bi, S, and Se. The EDS results of all these compounds are in agreement with the compositions obtained from the refinements of the crystal structure, Figure S2. The  $\text{Cs}_2\text{Ag}_{2.5}\text{Bi}_{8.5}\text{Se}_{15}$  was found in the products of the reaction performed to obtain  $\text{Cs}_{0.6}\text{Ag}_{0.8}\text{Bi}_{2.2}\text{Se}_4$  as an isostructural analog of  $\text{Cs}_{0.6}\text{Ag}_{0.8}\text{Bi}_{2.2}\text{S}_4$ .

Differential thermal analysis (DTA) of  $\text{Cs}_{0.6}\text{Ag}_{0.8}\text{Bi}_{2.2}\text{S}_4$  was conducted with a heating and cooling rate of  $10 \text{ }^\circ\text{C}/\text{min}$  to  $750 \text{ }^\circ\text{C}$  for two consecutive cycles. DTA revealed an endothermic peak at  $687 \text{ }^\circ\text{C}$  and one exothermic peak at  $688 \text{ }^\circ\text{C}$ , Figure 1(b). PXRD of the DTA-derived products showed that the compound melts congruently, Figure S3.  $\text{Cs}_{1.2}\text{Ag}_{0.6}\text{Bi}_{3.4}\text{S}_6$  is stable up to  $620 \text{ }^\circ\text{C}$  as indicated by DTA, Figure S4.

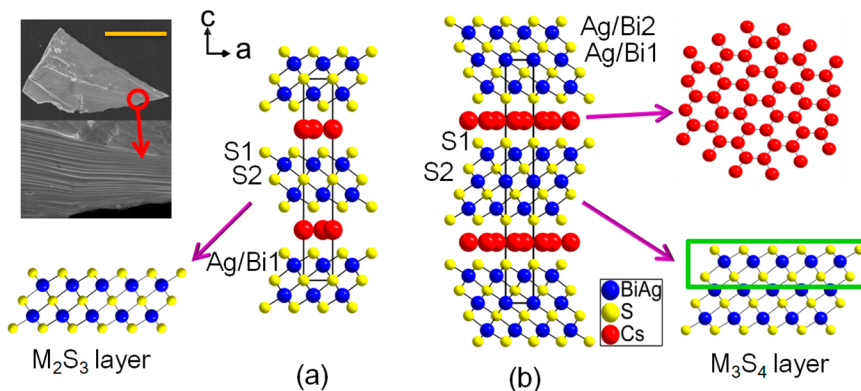
**Crystal Structures.**  $\text{Cs}_{1.2}\text{Ag}_{0.6}\text{Bi}_{3.4}\text{S}_6$ ,  $\text{Cs}_{1.2}\text{Ag}_{0.6}\text{Bi}_{3.4}\text{Se}_6$ ,  $\text{Cs}_{0.6}\text{Ag}_{0.8}\text{Bi}_{2.2}\text{S}_4$ , and  $\text{Cs}_2\text{Ag}_{2.5}\text{Bi}_{8.5}\text{Se}_{15}$  crystallize in three different structure types.  $\text{Cs}_{1.2}\text{Ag}_{0.6}\text{Bi}_{3.4}\text{S}_6$  and  $\text{Cs}_{1.2}\text{Ag}_{0.6}\text{Bi}_{3.4}\text{Se}_6$  are isostructural with the space group of  $P6_3/mmc$ , see Table 1. The unit cell of  $\text{Cs}_{1.2}\text{Ag}_{0.6}\text{Bi}_{3.4}\text{Se}_6$  is slightly larger than that of  $\text{Cs}_{1.2}\text{Ag}_{0.6}\text{Bi}_{3.4}\text{S}_6$  because of the larger radius of Se.<sup>61</sup> Herein, we describe in detail only the representative crystal structure of  $\text{Cs}_{1.2}\text{Ag}_{0.6}\text{Bi}_{3.4}\text{S}_6$ .  $\text{Cs}_{1.2}\text{Ag}_{0.6}\text{Bi}_{3.4}\text{S}_6$  consists of infinite anionic  $[\text{Ag}_x\text{Bi}_{2-x}\text{S}_3]_{n-2x}^{2-}$  quintuple slabs separated by  $\text{Cs}^+$  cations. SEM images show a step-like texture on the plate-like crystals of  $\text{Cs}_{1.2}\text{Ag}_{0.6}\text{Bi}_{3.4}\text{S}_6$  which arise from the stacking of the individual layers, Figure 2. There is only one crystallographic position for the Ag/Bi atoms. Each  $[\text{Ag}_x\text{Bi}_{2-x}\text{S}_3]_{n-2x}^{2-}$  slab is two octahedra thick, and they are isostructural to the layers of  $\text{Bi}_2\text{Se}_3$ , and has mixed occupancy of Ag/Bi1 (15% Ag and 85% Bi) octahedral sites bound to six sulfur atoms, Figure 2(a). The Ag/Bi–S bond distances range from  $2.62(2)$  to  $3.10(3) \text{ \AA}$ . The average Ag/Bi–S distance is  $2.830 \text{ \AA}$ , which is very similar to the Bi–S distances reported in  $\text{KBi}_{6.33}\text{S}_{10}$  and  $\text{K}_2\text{Bi}_3\text{S}_{13}$ .<sup>62</sup> The  $\text{Cs}^+$  cations partially occupy two different Wyckoff positions 2b and 2d making these ions highly disordered in the  $ab$ -plane.

The  $\text{Cs}_{1.2}\text{Ag}_{0.6}\text{Bi}_{3.4}\text{S}_6$  structure is similar to the  $\text{A}_x\text{Cd}_x\text{Bi}_{4-x}\text{Q}_6$  ( $\text{A} = \text{Cs, Rb, K}$ ;  $\text{Q} = \text{S}$ ;  $\text{A} = \text{Cs}$ ; and  $\text{Q} = \text{Se}$ ) compounds.<sup>46</sup> The  $\text{A}_x\text{Cd}_x\text{Bi}_{4-x}\text{Q}_6$  structure consists of infinite anionic  $[\text{Cd}_x\text{Bi}_{4-x}\text{S}_6]_n^{-x}$

**Table 1. Crystal Data and Structural Refinement Statistics for  $\text{Cs}_{1.2}\text{Ag}_{0.6}\text{Bi}_{3.4}\text{S}_6$ ,  $\text{Cs}_{1.2}\text{Ag}_{0.6}\text{Bi}_{3.4}\text{Se}_6$ ,  $\text{Cs}_{0.6}\text{Ag}_{0.8}\text{Bi}_{2.2}\text{S}_4$ , and  $\text{Cs}_2\text{Ag}_{2.5}\text{Bi}_{8.5}\text{Se}_{15}$  at 293(2) K<sup>a</sup>**

empirical formula	$\text{Cs}_{1.2}\text{Ag}_{0.6}\text{Bi}_{3.4}\text{S}_6$	$\text{Cs}_{1.2}\text{Ag}_{0.6}\text{Bi}_{3.4}\text{Se}_6$	$\text{Cs}_{0.6}\text{Ag}_{0.8}\text{Bi}_{2.2}\text{S}_4$	$\text{Cs}_2\text{Ag}_{2.5}\text{Bi}_{8.5}\text{Se}_{15}$
formula weight	1130.08	1399.95	754.05	3496.22
crystal system	hexagonal	hexagonal	hexagonal	orthorhombic
space group	$P6_3/mmc$	$P6_3/mmc$	$P6_3/mmc$	$Pnnm$
<i>a</i> (Å)	4.0300(14)	4.1456(8)	4.0331(6)	12.448(3)
<i>b</i> (Å)	4.0300(14)	4.1456(14)	4.0331(6)	32.342(6)
<i>c</i> (Å)	24.212(5)	25.449(5)	30.438(6)	4.1399(8)
volume (Å <sup>3</sup> )	340.5(2)	378.77(16)	428.77(15)	1666.7(6)
<i>Z</i>	1	1	2	2
density (calculated) (g/cm <sup>3</sup> )	5.510	6.137	5.840	6.967
absorption coefficient (mm <sup>-1</sup> )	48.635	57.705	50.229	64.656
<i>F</i> (000)	474	577	634	2886
crystal size (mm <sup>3</sup> )	0.2252 × 0.1041 × 0.0123	0.2945 × 0.1289 × 0.0013	0.1474 × 0.0945 × 0.009	0.1434 × 0.1206 × 0.0055
$\theta$ range for data collection (deg.)	1.682–29.043	3.202–24.900	4.017–24.981	1.753 to 23.498°
index ranges	$-4 \leq h \leq 5, -5 \leq k \leq 5, -33 \leq l \leq 33$	$-4 \leq h \leq 4, -4 \leq k \leq 4, -30 \leq l \leq 30$	$-4 \leq h \leq 4, -4 \leq k \leq 4, -36 \leq l \leq 35$	$-14 \leq h \leq 14, -38 \leq k \leq 38, -4 \leq l \leq 4$
reflections collected	2994	1847	2177	9867
independent reflections	227 [ $R_{\text{int}} = 0.0920$ ]	167 [ $R_{\text{int}} = 0.1872$ ]	190 [ $R_{\text{int}} = 0.0683$ ]	1428 [ $R_{\text{int}} = 0.1722$ ]
completeness to $\theta = 25.242^\circ$	100%	98.8%	97.4%	99.6%
refinement method	full-matrix least-squares on $F^2$			
goodness-of-fit	1.340	1.392	0.703	1.064
final <i>R</i> indices [ $>2\sigma(I)$ ]	$R_1 = 0.0594, wR_1 = 0.1096$	$R_1 = 0.0810, wR_1 = 0.1883$	$R_1 = 0.0447, wR_1 = 0.1233$	$R_1 = 0.0753, wR_1 = 0.1342$
<i>R</i> indices [all data]	$R_2 = 0.0638, wR_2 = 0.1113$	$R_2 = 0.0981, wR_2 = 0.1953$	$R_2 = 0.0491, wR_2 = 0.1299$	$R_2 = 0.1351, wR_2 = 0.1504$
largest diff. peak and hole (e·Å <sup>-3</sup> )	2.527 and -1.862	3.468 and -2.622	2.295 and -1.240	2.414 and -2.277

<sup>a</sup> $R = \sum \|F_o - |F_c\| \| / \sum |F_o\|$ ,  $wR = \{\sum [w(|F_o|^2 - |F_c|^2)^2] / \sum [w|F_o|^4]\}^{1/2}$  and  $w = 1 / [\sigma^2(F_o^2) + (22.2621P)]$  where  $P = (F_o^2 + 2F_c^2) / 3$ .

**Figure 2.** Crystal image (left), (a) the unit cell of  $\text{Cs}_{1.2}\text{Ag}_{0.6}\text{Bi}_{3.4}\text{S}_6$  and (b) the unit cell of  $\text{Cs}_{0.6}\text{Ag}_{0.8}\text{Bi}_{2.2}\text{S}_4$ . The scale bar is 100  $\mu\text{m}$ .

layers which adopt the hexagonal motif of the  $\text{Bi}_2\text{Se}_3$  structure type, separated by disordered Cs cations.  $\text{Cs}_{1.2}\text{Ag}_{0.6}\text{Bi}_{3.4}\text{S}_6$  is derived from  $\text{A}_x\text{Cd}_x\text{Bi}_{4-x}\text{Q}_6$  by changing the six coordinated  $\text{Cd}^{2+}$  to  $\text{Ag}^+$  with the extra negative charge balanced by accommodating more alkali metals between the layers, i.e.,  $\text{A}_{2x}\text{Ag}_x\text{Bi}_{4-x}\text{Q}_6$ .

$\text{Cs}_{0.6}\text{Ag}_{0.8}\text{Bi}_{2.2}\text{S}_4$  also adopts the  $P6_3/mmc$  space group, see Table 1. The structure is composed of  $[\text{Ag}_x\text{Bi}_{3-x}\text{S}_4]_n$  slabs and disordered  $\text{Cs}^+$  cations. These slabs are thicker than the  $[\text{Ag}_x\text{Bi}_{2-x}\text{S}_3]_{n-2}$  layer described above. In comparison, the unit cell parameters along *a* and *b* directions of  $\text{Cs}_{0.6}\text{Ag}_{0.8}\text{Bi}_{2.2}\text{S}_4$  are the same as that of  $\text{Cs}_{1.2}\text{Ag}_{0.6}\text{Bi}_{3.4}\text{S}_6$  but the *c*-axis of  $\text{Cs}_{0.6}\text{Ag}_{0.8}\text{Bi}_{2.2}\text{S}_4$  is lengthened by 6.223 Å compared to  $\text{Cs}_{1.2}\text{Ag}_{0.6}\text{Bi}_{3.4}\text{S}_6$ . Figure 2(b) shows how adding a layer of  $[\text{Ag}/\text{BiS}]_n$  atoms to the  $[\text{Ag}_x\text{Bi}_{2-x}\text{S}_3]_n$  slab leads to the thicker  $[\text{Ag}_x\text{Bi}_{3-x}\text{S}_4]_n$  slab. The  $[\text{Ag}_x\text{Bi}_{3-x}\text{S}_4]_n$  are three octahedra thick, and feature two crystallographically different Ag/Bi sites 2a and 4f. The  $\text{Ag}/\text{Bi}_1$  (58% Bi and 42% Ag) site forms regular octahedral coordination with  $\text{Ag}/\text{Bi}_1-\text{S}_2$  distances of 2.818(6) Å. The  $\text{Ag}/\text{Bi}_2$  (82% Bi and

18% Ag) site has three long  $\text{Ag}/\text{Bi}_2-\text{S}_2$  and three short  $\text{Ag}/\text{Bi}_2-\text{S}_1$  bonds with an average bond distance of 2.891 Å. The Cs cation layer resembles that observed in  $\text{Cs}_{1.2}\text{Ag}_{0.6}\text{Bi}_{3.4}\text{S}_6$ .

$\text{Cs}_2\text{Ag}_{2.5}\text{Bi}_{8.5}\text{Se}_{15}$  adopts the  $Pnnm$  space group, and its structure belongs to the  $\text{A}_2[\text{M}_{5+n}\text{Se}_{9+n}]$  homology with  $n = 6$ .<sup>63</sup> The  $n = 1, 2, 3, 4$  members of the series were reported previously.<sup>63</sup> The discovery of  $\text{Cs}_2\text{Ag}_{2.5}\text{Bi}_{8.5}\text{Se}_{15}$  validates the predictive function of the homologous series. In terms of the homology it can be expressed as  $\text{Cs}_2[(\text{Ag}/\text{Bi})_{11}\text{Se}_{15}]$  featuring the  $[\text{M}_{11}\text{Se}_{15}]^{2-}$  ( $\text{M} = \text{Ag}/\text{Bi}$ ) modules, Figure 3(b). This module is four “ $\text{BiSe}_6$ ” octahedra wide and three octahedra thick, and is propagated by linking with identical neighboring modules through sharing an edge of the  $\text{Ag}/\text{Bi}-\text{Se}$  octahedron to form a stepwise slab. The structure has six crystallographically different Ag/Bi atoms. With the exception of Bi1, all metal sites have mixed occupancy by Bi and Ag.  $\text{Ag}/\text{Bi}_6$  forms a regular octahedron and other Ag/Bi atoms are in distorted octahedral coordination environments. The bond distances of  $\text{Ag}/\text{Bi}-\text{Se}$  vary from 2.780(5) to 3.194(5) Å with

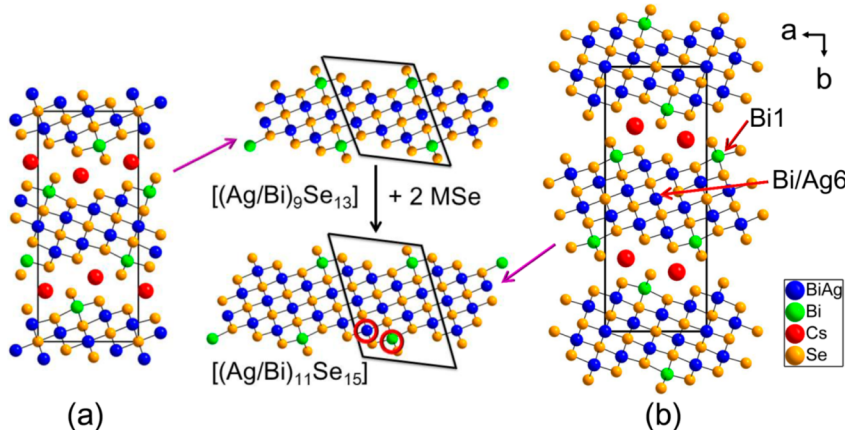


Figure 3. Unit cell of (a)  $\text{Cs}_2\text{Ag}_{1.5}\text{Bi}_{7.5}\text{Se}_{13}$  and (b)  $\text{Cs}_2\text{Ag}_{2.5}\text{Bi}_{8.5}\text{Se}_{15}$  and the evolution of the layers (middle).

an average Ag/Bi–Se distance of 2.941 Å. The  $\text{Cs}^+$  cations are in a bicapped trigonal prismatic coordination with  $\text{Cs}$ –Se distances range between 3.579(7) and 3.579(7) Å.<sup>63</sup>

Homologous series of compounds are families of related structures that are composed of similar building blocks whose number increases by regular increments. Homologous series provide an ideal playground to predict new materials.<sup>27,32</sup> These structural characteristics make it possible to manipulate the physical properties through a controlled modification of the crystal structure and/or chemical composition.<sup>64</sup> These compounds with flat layers intercalated with  $\text{Cs}^+$  cations can be summarized into a new homologous series  $\text{A}_x[\text{M}_m\text{Q}_{1+m}]$  ( $\text{Q} = \text{S}$  and  $\text{Se}$ ).  $\text{K}_{2x}\text{Mn}_x\text{Sn}_{3-x}\text{S}_6$  (KMS-1),<sup>65</sup>  $\text{K}_{2x}\text{Mg}_x\text{Sn}_{3-x}\text{S}_6$  (KMS-2)<sup>66</sup> and  $\text{RbBiS}_2$ <sup>67</sup> contain  $[\text{MS}_2]$  monolayers.  $\text{K}_{2x}\text{Mn}_x\text{Sn}_{3-x}\text{S}_6$  and  $\text{K}_{2x}\text{Mg}_x\text{Sn}_{3-x}\text{S}_6$  can be denoted as  $\text{K}_{2x/3}(\text{M}/\text{Sn})\text{S}_2$  ( $\text{M} = \text{Mn}$  and  $\text{Mg}$ ) with  $m = 1$ . The monolayer in KMS-1 and KMS-2 derives from the simplest of octahedral layers  $\text{SnS}_2$  by substituting some  $\text{Sn}^{4+}$  atoms for divalent  $\text{Mg}^{2+}$  and  $\text{Mn}^{2+}$  atoms with the resulting negative charge being balanced by  $\text{K}^+$  atoms.  $\text{Cs}_{1.2}\text{Ag}_{0.6}\text{Bi}_{3.4}\text{Q}_6$  and  $\text{Cs}_x\text{Cd}_x\text{Bi}_{4-x}\text{Q}_6$  ( $\text{Q} = \text{S}$ ,  $\text{Se}$ ) can be denoted as  $\text{A}_x(\text{M}/\text{Bi})_2\text{Q}_3$  ( $m = 2$ ) with structure possessing  $[\text{M}_2\text{Q}_3]$  double octahedral layers.<sup>67</sup>  $\text{Cs}_{0.6}\text{Ag}_{0.8}\text{Bi}_{2.2}\text{S}_4$  possesses  $[\text{M}_3\text{S}_4]_n$  triple octahedral layer with  $m = 3$ .  $[\text{M}_3\text{S}_4]_n$  layers are also found in the three-dimensional  $\text{PbBi}_2\text{Se}_4$  compound which is a member of the galenobismuthite homologous series.<sup>38</sup>  $\text{Cs}_{0.6}\text{Ag}_{0.8}\text{Bi}_{2.2}\text{S}_4$  can be derived from a  $[\text{PbBi}_2\text{Se}_4]$  slab by substituting  $\text{Pb}^{2+}$  atoms with  $\text{Ag}^+$ . This renders the slab negatively charged and the  $\text{Cs}^+$  balance the charge by residing between the layers.

**Optical Absorption and Electronic Structure Calculations.** The four title compounds are semiconductors as indicated by the solid state electronic absorption spectra which reveal the presence of bandgaps.  $\text{Cs}_{1.2}\text{Ag}_{0.6}\text{Bi}_{3.4}\text{S}_6$  shows a sharp and strong optical absorption edge at 1.20 eV, Figure 4.  $\text{Cs}_{0.6}\text{Ag}_{0.8}\text{Bi}_{2.2}\text{S}_4$  shows a smaller band gap (1.09 eV) than  $\text{Cs}_{1.2}\text{Ag}_{0.6}\text{Bi}_{3.4}\text{S}_6$  due to the thicker layer.  $\text{Cs}_{1.2}\text{Ag}_{0.6}\text{Bi}_{3.4}\text{Se}_6$  possesses a band gap of 0.67 eV.  $\text{Cs}_2\text{Ag}_{2.5}\text{Bi}_{7.5}\text{Se}_{15}$  has the smallest band gap of 0.65 eV.

The DFT calculated electronic structures indicate an indirect band gap of 0.51 eV for  $\text{CsAgBi}_2\text{S}_4$  and a direct band gap of 0.21 eV for  $\text{Cs}_2\text{AgBi}_3\text{S}_6$ , see Figure 5. This underestimation of the calculated bandgaps compared to experiment is a well-known tendency of semilocal exchange-correlation functionals like PBE.<sup>68,69</sup>

**Ion-Exchange Chemistry.** The interlayer space available for the disordered  $\text{Cs}^+$  cations in  $\text{Cs}_{1.2}\text{Ag}_{0.6}\text{Bi}_{3.4}\text{S}_6$  and  $\text{Cs}_{0.6}\text{Ag}_{0.8}\text{Bi}_{2.2}\text{S}_4$  with their weak ionic interactions, gives ample room

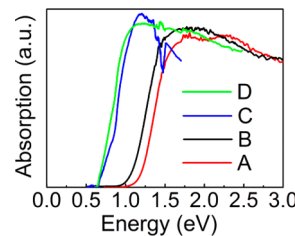


Figure 4. Band gaps of A:  $\text{Cs}_{1.2}\text{Ag}_{0.6}\text{Bi}_{3.4}\text{S}_6$  with  $E_g = 1.20$  eV; B:  $\text{Cs}_{0.6}\text{Ag}_{0.8}\text{Bi}_{2.2}\text{S}_4$  with  $E_g = 1.09$  eV; C:  $\text{Cs}_{1.2}\text{Ag}_{0.6}\text{Bi}_{3.4}\text{Se}_6$  with  $E_g = 0.67$  eV; and D:  $\text{Cs}_2\text{Ag}_{2.5}\text{Bi}_{7.5}\text{Se}_{15}$  with  $E_g = 0.65$  eV.

for ion mobility and this suggested to us that these atoms could participate in ion-exchange reactions with other cations. In fact, the study of metal sulfide as ion-exchangers is an emerging field and promises materials with unique applications.<sup>70</sup> We find that

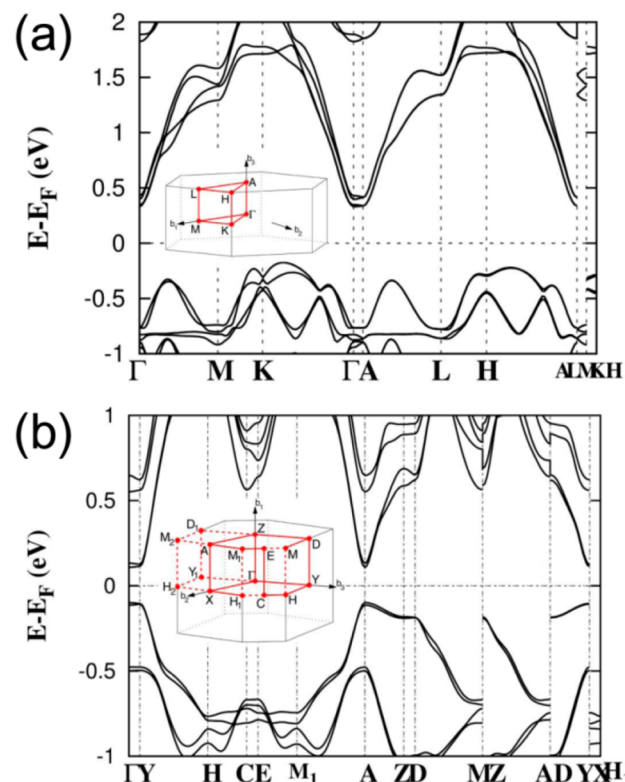


Figure 5. Electronic band structure of  $\text{CsAgBi}_2\text{S}_4$  (a) and  $\text{Cs}_2\text{AgBi}_3\text{S}_6$  (b).

when these two compounds are immersed in a water solution of  $\text{Ag}^+$ ,  $\text{Cd}^{2+}$ ,  $\text{Co}^{2+}$ ,  $\text{Pb}^{2+}$ , and  $\text{Zn}^{2+}$  ions for 24 h the ion-exchange proceeds with apparent ease. Table 2 lists the EDS elemental

**Table 2. Energy-Dispersive X-ray Spectroscopy (EDS) Elemental Analyses Results of Ion-Exchange Products**

	Cs	X*	Ag	Bi	S
$\text{Cs}_{1.2}\text{Ag}_{0.6}\text{Bi}_{3.4}\text{S}_6$					
As-synthesized	0.92		0.70	3.20	6
Ag-exchanged			10.74	0.41	6
Cd-exchanged		0.32	0.68	3.20	6
Co-exchanged	0.20	0.50	0.62	3.40	6
Pb-exchanged		0.50	0.62	4.00	6
Zn-exchanged		0.40	0.70	3.00	6
$\text{Cs}_{0.6}\text{Ag}_{0.8}\text{Bi}_{2.2}\text{S}_4$					
As-synthesized	0.94		0.56	2.24	4
Ag-exchanged			1.23	2.49	4
Cd-exchanged		0.30	0.60	2.70	4
Co-exchanged	0.02	0.12	0.64	2.11	4
Pb-exchanged		0.20	0.82	2.30	4
Zn-exchanged		0.21	0.75	2.14	4

\*X\* = Ag, Cd, Co, Pb, and Zn cations, correspondingly.

analysis results of the materials after ion exchange. The table shows that in  $\text{Cs}_{1.2}\text{Ag}_{0.6}\text{Bi}_{3.4}\text{S}_6$ , the  $\text{Cs}^+$  can be completely replaced by  $\text{Cd}^{2+}$ ,  $\text{Pb}^{2+}$ , and  $\text{Zn}^{2+}$  and most exchanged by  $\text{Co}^{2+}$  and the exchanged cations distribute homogeneously in the layered crystal, Figure S5. In the case of  $\text{Cs}_{0.6}\text{Ag}_{0.8}\text{Bi}_{2.2}\text{S}_4$  the  $\text{Cs}^+$  cations can be completely exchanged by  $\text{Ag}^+$ ,  $\text{Cd}^{2+}$ ,  $\text{Co}^{2+}$ ,  $\text{Pb}^{2+}$ , and  $\text{Zn}^{2+}$ , Figure S6. The ion-exchange process is illustrated in Figure 6, and

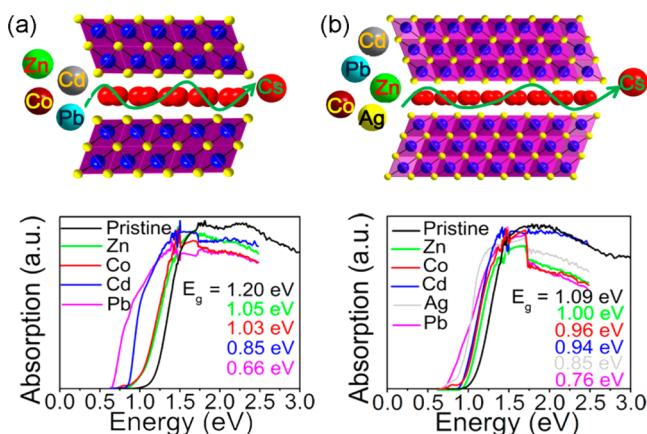


**Figure 6.** Ion-exchange mechanism and band gap changes after ion exchange (a)  $\text{Cs}_{1.2}\text{Ag}_{0.6}\text{Bi}_{3.4}\text{S}_6$  and (b)  $\text{Cs}_{0.6}\text{Ag}_{0.8}\text{Bi}_{2.2}\text{S}_4$ .

the ion exchange was further confirmed by the shift of the PXRD peaks, i.e., (002), which are shown in Figure 7. Taking  $\text{Pb}^{2+}$  as an example, after ion exchange, the (002) basal peak moved to higher angles, indicating a decrease of the interlayer distance as a result of ion exchange which is consistent with the smaller size of  $\text{Pb}^{2+}$  than  $\text{Cs}^+$ .

The process of ion exchange can be described by the following equations:

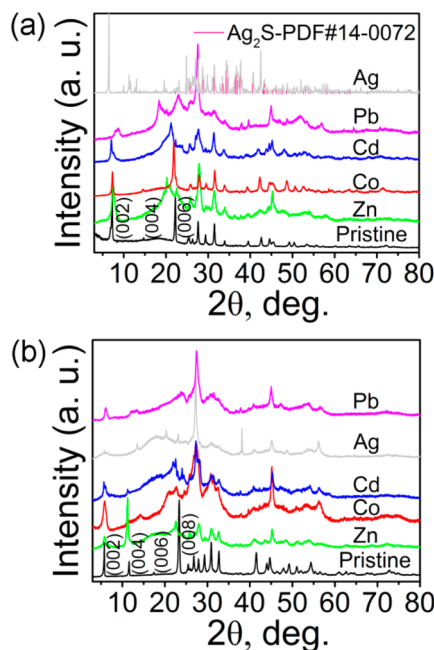
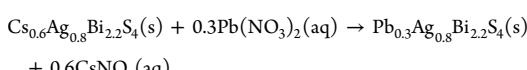
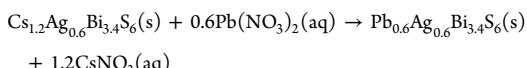


**Figure 7.** (a) The PXRD of  $\text{Cs}_{1.2}\text{Ag}_{0.6}\text{Bi}_{3.4}\text{S}_6$  before and after ion exchange; and (b) the PXRD of  $\text{Cs}_{0.6}\text{Ag}_{0.8}\text{Bi}_{2.2}\text{S}_4$  before and after ion exchange.

It is characteristic that the ion-exchange process results in materials with a red-shifted optical absorption. The  $\text{Pb}^{2+}$  exchanged materials of both  $\text{Cs}_{1.2}\text{Ag}_{0.6}\text{Bi}_{3.4}\text{S}_6$  and  $\text{Cs}_{0.6}\text{Ag}_{0.8}\text{Bi}_{2.2}\text{S}_4$  show the largest red shift and thus smallest band gaps of 0.66 and 0.76 eV, respectively. This large band gap narrowing is due to the inter layer bonding change from ionic in  $\text{Cs}^+ \cdots \text{S}^2-$  to covalent in Pb-S so the structure becomes more three-dimensional.<sup>71</sup> When the  $\text{Cs}^+$  in  $\text{Cs}_{1.2}\text{Ag}_{0.6}\text{Bi}_{3.4}\text{S}_6$  are ion exchanged with  $\text{Zn}^{2+}$ ,  $\text{Cd}^{2+}$ , and  $\text{Co}^{2+}$  the band gap also narrows from 1.20 eV of the pristine sample to 1.05, 1.03, and 0.85 eV, respectively. When immersed in solution of  $\text{Ag}^+$  PXRD measurements reveal that  $\text{Cs}_{1.2}\text{Ag}_{0.6}\text{Bi}_{3.4}\text{S}_6$  decomposes partially to  $\text{Ag}_2\text{S}$  after ion exchange, Figure 7(a). This is attributed to the great thermodynamic and kinetic stability of the  $\text{Ag}_2\text{S}$  phase. The  $\text{Cs}^+$  in  $\text{Cs}_{0.6}\text{Ag}_{0.8}\text{Bi}_{2.2}\text{S}_4$  can be ion exchanged with  $\text{Zn}^{2+}$ ,  $\text{Co}^{2+}$ ,  $\text{Cd}^{2+}$ , and  $\text{Ag}^+$  resulting in band gaps of 1.00, 0.96, 0.94, 0.85, and 0.76 eV, respectively. Unlike in  $\text{Cs}_{1.2}\text{Ag}_{0.6}\text{Bi}_{3.4}\text{S}_6$ , no  $\text{Ag}_2\text{S}$  was observed in the case of  $\text{Cs}_{0.6}\text{Ag}_{0.8}\text{Bi}_{2.2}\text{S}_4$  under the same ion exchange conditions, Figure 6(b). Both  $\text{Cs}_{1.2}\text{Ag}_{0.6}\text{Bi}_{3.4}\text{S}_6$  and  $\text{Cs}_{0.6}\text{Ag}_{0.8}\text{Bi}_{2.2}\text{S}_4$  exhibit partial ion exchange in  $\text{Co}^{2+}$  solution giving products with formula (derived by EDS) of  $\text{Cs}_{0.20}\text{Co}_{0.50}\text{Ag}_{0.26}\text{Bi}_{3.40}\text{S}_6$  and  $\text{Cs}_{0.02}\text{Co}_{0.12}\text{Ag}_{0.64}\text{Bi}_{2.11}\text{S}_4$ , respectively. The ion exchange process provides a direct “soft chemistry” route to new compounds which are not readily accessible by traditional solid state synthesis techniques.

**Electrical and Thermal Transport Properties.**  $\text{Cs}_{1.2}\text{Ag}_{0.6}\text{Bi}_{3.4}\text{S}_6$  features a low electrical conductivity ( $<1 \text{ S} \cdot \text{cm}^{-1}$ ) and a relatively high Seebeck coefficient ( $-440 \mu\text{V} \cdot \text{K}^{-1}$ ) at room temperature, which suggests a relatively low carrier concentration, Figure 8(a, b). With increasing temperature, the electrical conductivity rises rapidly while the absolute value of Seebeck coefficient decreases, indicating semiconducting transport behavior, with the highest electrical conductivity of  $11 \text{ S} \cdot \text{cm}^{-1}$ , and the Seebeck coefficient of  $-183 \mu\text{V} \cdot \text{K}^{-1}$  at 775 K. The Seebeck coefficients are negative in the entire temperature range, suggesting electrons as the majority carriers. The conductivity of  $\text{Cs}_{0.6}\text{Ag}_{0.8}\text{Bi}_{2.2}\text{S}_4$  is  $0.05 \text{ S} \cdot \text{cm}^{-1}$  and the Seebeck coefficient is

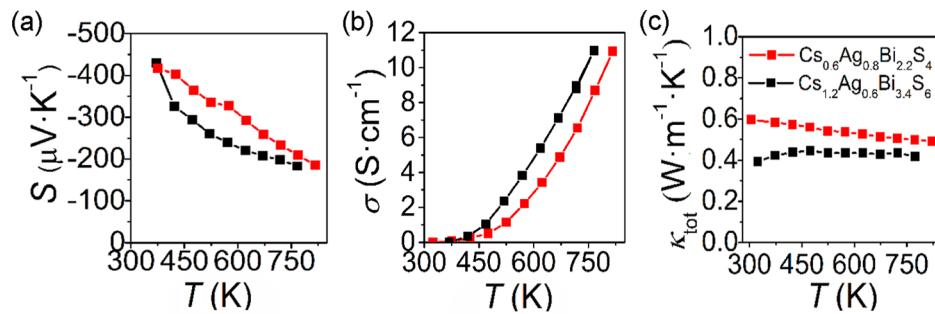


**Figure 8.** (a) Electrical conductivity, (b) Seebeck coefficient, and (c) thermal conductivity values as a function of temperature for  $\text{Cs}_{1.2}\text{Ag}_{0.6}\text{Bi}_{3.4}\text{S}_6$  (black) and  $\text{Cs}_{0.6}\text{Ag}_{0.8}\text{Bi}_{2.2}\text{S}_4$  (red).

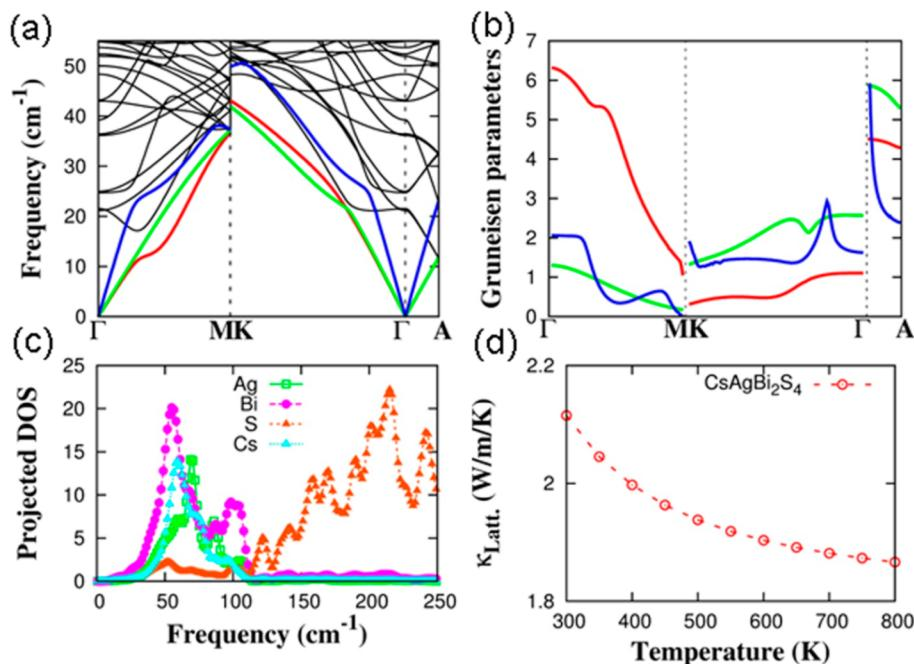


**Figure 9.** (a) Phonon and (b) Grüneisen dispersions for  $\text{CsAgBi}_2\text{S}_4$ . (c) The projected phonon density of states for  $\text{CsAgBi}_2\text{S}_4$ . (d) The temperature dependent lattice thermal conductivities of  $\text{CsAgBi}_2\text{S}_4$ , calculated by the Debye–Callaway model.

relatively large with  $-432 \mu\text{V}\cdot\text{K}^{-1}$  at 373 K. When heating both electrical conductivity and Seebeck coefficient have the same trend as that of  $\text{Cs}_{1.2}\text{Ag}_{0.6}\text{Bi}_{3.4}\text{S}_6$  with the highest conductivity of  $11 \text{ S}\cdot\text{cm}^{-1}$  and Seebeck coefficient of  $-185 \mu\text{V}\cdot\text{K}^{-1}$  at 820 K.

Another noteworthy feature of  $\text{Cs}_{1.2}\text{Ag}_{0.6}\text{Bi}_{3.4}\text{S}_6$  is its ultralow thermal conductivity of  $\sim 0.45 \text{ W}\cdot\text{m}^{-1}\cdot\text{K}^{-1}$  at 300 K, Figure 8(c). Moreover, the thermal conductivity shows very weak temperature dependence. This low value is comparable to compounds known for their ultralow thermal conductivity and excellent thermoelectric performance, i.e.,  $\text{Cu}_{2-x}\text{Se}$  ( $0.66\text{--}1.1 \text{ W}\cdot\text{m}^{-1}\cdot\text{K}^{-1}$ ),<sup>72</sup>  $\text{Cu}_{2-x}\text{S}$  ( $0.25\text{--}0.6 \text{ W}\cdot\text{m}^{-1}\cdot\text{K}^{-1}$ ),<sup>73</sup>  $\text{AgSbSe}_2$  ( $0.23\text{--}0.4 \text{ W}\cdot\text{m}^{-1}\cdot\text{K}^{-1}$ ),<sup>74</sup>  $\text{CsAg}_5\text{Te}_3$  ( $0.18\text{--}0.14 \text{ W}\cdot\text{m}^{-1}\cdot\text{K}^{-1}$ ),<sup>75</sup> and so forth.  $\text{Cs}_{0.6}\text{Ag}_{0.8}\text{Bi}_{2.2}\text{S}_4$  also possesses a low thermal conductivity of  $0.6 \text{ W}\cdot\text{m}^{-1}\cdot\text{K}^{-1}$  at room temperature, Figure 8(c). It decreases with increasing temperature with the lowest value of  $0.49 \text{ W}\cdot\text{m}^{-1}\cdot\text{K}^{-1}$  at 825 K. The origin of this ultralow thermal conductivity could be related to its layered structure and the disordered Cs ion distribution that lends them to “rattle”. Rattler atoms have been invoked as phonon scattering centers in many compounds including  $\text{Cs}_2\text{Hg}_6\text{S}_7$ ,<sup>76</sup>  $\text{Ba}_8\text{Au}_{16}\text{P}_{30}$ ,<sup>77</sup>  $\text{CsAg}_5\text{Te}_3$ ,<sup>75</sup> Skutterudites,<sup>78–82</sup> and recently in a family of  $\text{Ba}_2\text{AuBi}$  and related Heusler compounds.<sup>83</sup>

To understand the origin of the low thermal conductivity of  $\text{CsAgBi}_2\text{S}_4$ , the phonon dispersions and Grüneisen dispersions were calculated by using DFT. Grüneisen parameters can characterize the relationship between phonon frequency and crystal volume change, thus provide an insight into the lattice anharmonicity.<sup>60,75</sup> The Grüneisen parameters for the acoustic modes in  $\text{CsAgBi}_2\text{S}_4$  are all large and give rise to large average acoustic Grüneisen parameters of  $\gamma_{\text{TA}} = 2.87$ ,  $\gamma_{\text{TA}'} = 2.07$ ,  $\gamma_{\text{LA}} = 1.61$ , Figure 9a, b. Thus, the Grüneisen parameters of  $\text{CsAgBi}_2\text{S}_4$  indicate strongly anharmonic vibrational properties. The low frequency vibration modes originate from the Cs, Ag, and Bi contributions which exhibit a rattler-like behavior. These modes are identified as three low frequency peaks in Figure 9c. Similar to  $\text{CsAg}_5\text{Te}_3$ , where the concerted rattling modes account for the low lattice thermal conductivity,<sup>75</sup> rattling vibrations in  $\text{CsAgBi}_2\text{S}_4$  contribute strongly to suppressing the lattice thermal conductivity. On the basis of the phonon dispersions and Grüneisen parameters, the calculated lattice thermal conductivities (calculated via a Debye–Grüneisen model) of  $\text{CsAgBi}_2\text{S}_4$  are shown in Figure 9d. The calculated value is about  $2.1 \text{ W}\cdot\text{m}^{-1}\cdot\text{K}^{-1}$  at 300 K, which is significantly larger than the measurements of total thermal conductivity around  $0.6 \text{ W}\cdot\text{m}^{-1}\cdot\text{K}^{-1}$  for  $\text{Cs}_{0.6}\text{Ag}_{0.8}\text{Bi}_{2.2}\text{S}_4$ . On the one hand,

the discrepancy could be due to the difference in composition between the calculated ideal structure of  $\text{CsAgBi}_2\text{S}_4$  and the experimentally determined one at  $\text{Cs}_{0.6}\text{Ag}_{0.8}\text{Bi}_{2.2}\text{S}_4$ , which is really difficult to represent by a simple supercell (due to the disorder-linked mixed occupancy of Cs). This discrepancy suggests the presence of extra phonon scattering induced by the disorder in the Cs layers and the mixed occupancy disorder of Bi in Ag which are not considered in our calculations.

## CONCLUSIONS

$\text{Cs}_{1.2}\text{Ag}_{0.6}\text{Bi}_{3.4}\text{S}_6$ ,  $\text{Cs}_{1.2}\text{Ag}_{0.6}\text{Bi}_{3.4}\text{Se}_6$ , and  $\text{Cs}_{0.6}\text{Ag}_{0.8}\text{Bi}_{2.2}\text{S}_4$  together with other reported compounds which possess flat  $\text{MSe}_6$  octahedral layers form a new homologous series  $\text{A}_x[\text{M}_m\text{Q}_{1+m}]$  ( $\text{Q} = \text{S}$  and  $\text{Se}$ ). In the context of this homology,  $\text{Cs}_{1.2}\text{Ag}_{0.6}\text{Bi}_{3.4}\text{S}_6$ ,  $\text{Cs}_{1.2}\text{Ag}_{0.6}\text{Bi}_{3.4}\text{Se}_6$ , and  $\text{Cs}_{0.6}\text{Ag}_{0.8}\text{Bi}_{2.2}\text{S}_4$  can be denoted as  $\text{Cs}_{0.6}(\text{Ag/Bi})_2\text{S}_3$  with  $m = 2$ ,  $\text{Cs}_{0.6}(\text{Ag/Bi})_2\text{Se}_3$  with  $m = 2$  and  $\text{Cs}_{0.6}(\text{Ag/Bi})_3\text{S}_4$  with  $m = 3$ , respectively. The  $\text{Cs}_2\text{Ag}_{2.5}\text{Bi}_{7.5}\text{Se}_{15}$  is new member of the known  $\text{A}_2[\text{M}_{5+n}\text{Se}_{9+n}]$  homology with  $n = 6$  and its synthesis enlarges this homologous family and inspires the pursuit of additional new members. The  $\text{Cs}^+$  ions intercalated between the layers of  $\text{Cs}_{1.2}\text{Ag}_{0.6}\text{Bi}_{3.4}\text{S}_6$  and  $\text{Cs}_{0.6}\text{Ag}_{0.8}\text{Bi}_{2.2}\text{S}_4$  structure can be topotactically exchanged with  $\text{Ag}^+$ ,  $\text{Cd}^{2+}$ ,  $\text{Co}^{2+}$ ,  $\text{Pb}^{2+}$ , and  $\text{Zn}^{2+}$  at room temperature to give new compound red-shifted band gaps tunable from 1.20 to 0.66 eV. Thermal conductivity measurements show that both  $\text{Cs}_{1.2}\text{Ag}_{0.6}\text{Bi}_{3.4}\text{S}_6$  and  $\text{Cs}_{0.6}\text{Ag}_{0.8}\text{Bi}_{2.2}\text{S}_4$  compounds possess extremely low thermal conductivity. Although a full study of the thermoelectric properties is not the focus of this paper, future systematic doping studies should explore their potential as high performance materials.

## ASSOCIATED CONTENT

### Supporting Information

The Supporting Information is available free of charge on the ACS Publications website at DOI: [10.1021/jacs.7b06373](https://doi.org/10.1021/jacs.7b06373).

Tables of atomic coordinates and displacement parameters of  $\text{Cs}_{1.2}\text{Ag}_{0.6}\text{Bi}_{3.4}\text{S}_6$ ,  $\text{Cs}_{1.2}\text{Ag}_{0.6}\text{Bi}_{3.4}\text{Se}_6$ ,  $\text{Cs}_{0.6}\text{Ag}_{0.8}\text{Bi}_{2.2}\text{S}_4$  and  $\text{Cs}_2\text{Ag}_{2.5}\text{Bi}_{8.5}\text{Se}_{15}$ ; SEM image and Energy-dispersive X-ray spectroscopy spectrum; PXRD after DTA (PDF)  
 X-ray and crystallographic data of  $\text{Cs}_{1.2}\text{Ag}_{0.6}\text{Bi}_{3.4}\text{S}_6$  (CIF)  
 X-ray and crystallographic data of  $\text{Cs}_{1.2}\text{Ag}_{0.6}\text{Bi}_{3.4}\text{Se}_6$  (CIF)  
 X-ray and crystallographic data of  $\text{Cs}_{0.6}\text{Ag}_{0.8}\text{Bi}_{2.2}\text{S}_4$  and  $\text{Cs}_2\text{Ag}_{2.5}\text{Bi}_{8.5}\text{Se}_{15}$  (CIF)  
 X-ray and crystallographic data of  $\text{Cs}_2\text{Ag}_{1.5}\text{Bi}_{7.5}\text{Se}_{15}$  (CIF)

## AUTHOR INFORMATION

### Corresponding Author

\*[m-kanatzidis@northwestern.edu](mailto:m-kanatzidis@northwestern.edu)

### ORCID

Jing Zhao: [0000-0002-8000-5973](https://orcid.org/0000-0002-8000-5973)

Gangjian Tan: [0000-0002-9087-4048](https://orcid.org/0000-0002-9087-4048)

Constantinos C. Stoumpos: [0000-0001-8396-9578](https://orcid.org/0000-0001-8396-9578)

Chris Wolverton: [0000-0003-2248-474X](https://orcid.org/0000-0003-2248-474X)

Haijie Chen: [0000-0003-3567-1763](https://orcid.org/0000-0003-3567-1763)

Mercouri G. Kanatzidis: [0000-0003-2037-4168](https://orcid.org/0000-0003-2037-4168)

### Author Contributions

All authors have given approval to the final version of the manuscript.

### Notes

The authors declare no competing financial interest.

## ACKNOWLEDGMENTS

This work was supported in part by National Science Foundation (Grant DMR-1708254). This work made use of the EPIC facility (NUANCE Center-Northwestern University), which has received support under the State of Illinois, Northwestern University, and the National Science Foundation with grants DMR-1121262 through the MRSEC program at the Materials Research Center, and EEC-0118025/003 through The Nanoscale Science and Engineering Center. S.H. and C.W. (DFT calculations) acknowledge support from the Department of Energy, Office of Science Basic Energy Sciences, under grant DE-SC0014520. This work was supported in part by a grant from the National Science Foundation of China (No. 51702329).

## REFERENCES

- Hulliger, F. *Structural Chemistry of Layer-Type Phases*; Lévy, F., Eds.; Springer: Netherlands, 1976.
- Kanatzidis, M. G. *Inorg. Chem.* **2017**, *56*, 3158.
- Kanatzidis, M. G. *Phosphorus, Sulfur Silicon Relat. Elem.* **1994**, *93*, 159.
- (a) Kanatzidis, M. G. *Acc. Chem. Res.* **2005**, *38*, 359. (b) Mrotzek, A.; Kanatzidis, MG *Acc. Chem. Res.* **2003**, *36*, 111.
- Besse, R.; Sabino, F. P.; Da Silva, J. L. F. *Phys. Rev. B: Condens. Matter Mater. Phys.* **2016**, *93*, 165205.
- (a) Androulakis, J.; Peter, S. C.; Li, H.; Malliakas, C. D.; Peters, J. A.; Liu, Z. F.; Wessels, B. W.; Song, J. H.; Jin, H.; Freeman, A. J.; Kanatzidis, M. G. *Adv. Mater.* **2011**, *23*, 4163. (b) Chung, I.; Malliakas, C. D.; Jang, J. I.; Canlas, C. G.; Weliky, D. P.; Kanatzidis, M. G. *J. Am. Chem. Soc.* **2007**, *129*, 14996. (c) Fang, L.; Im, J.; Stoumpos, C. C.; Shi, F. Y.; David, V.; Leroux, M.; Freeman, A. J.; Kwok, W. K.; Chung, D. Y.; Kanatzidis, M. *J. Am. Chem. Soc.* **2015**, *137*, 2311.
- Manos, M. J.; Kanatzidis, M. G. *J. Am. Chem. Soc.* **2009**, *131*, 6599.
- Banerjee, S.; Malliakas, C. D.; Kanatzidis, M. G. *Inorg. Chem.* **2012**, *51*, 11562.
- Zhao, S.; Gong, P.; Luo, S.; Liu, S.; Li, L.; Asghar, M. A.; Khan, T.; Hong, M.; Lin, Z.; Luo, J. *J. Am. Chem. Soc.* **2015**, *137*, 2207.
- Mannix, A. J.; Kiraly, B.; Hersam, M. C.; Guisinger, N. P. *Nat. Rev. Chem.* **2017**, *1*, 0014.
- Liu, Y.; Tang, M.; Meng, M.; Wang, M.; Wu, J.; Yin, J.; Zhou, Y.; Guo, Y.; Tan, C.; Dang, W. *Small* **2017**, *13*, 1603572.
- Zhang, Y.; He, K.; Chang, C.-Z.; Song, C.-L.; Wang, L.-L.; Chen, X.; Jia, J.-F.; Fang, Z.; Dai, X.; Shan, W.-Y.; Shen, S.-Q.; Niu, Q.; Qi, X.-L.; Zhang, S.-C.; Ma, X.-C.; Xue, Q.-K. *Nat. Phys.* **2010**, *6*, 584.
- Zhang, H.; Liu, C.-X.; Qi, X.-L.; Dai, X.; Fang, Z.; Zhang, S.-C. *Nat. Phys.* **2009**, *5*, 438.
- Venkatasubramanian, R.; Siivola, E.; Colpitts, T.; O'Quinn, B. *Nature* **2001**, *413*, 597.
- Xu, B.; Feng, T.; Agne, M. T.; Zhou, L.; Ruan, X.; Snyder, G. J.; Wu, Y. *Angew. Chem.* **2017**, *129*, 3600.
- Hong, M.; Chasapis, T. C.; Chen, Z.-G.; Yang, L.; Kanatzidis, M. G.; Snyder, G. J.; Zou, J. *ACS Nano* **2016**, *10*, 4719.
- Axtell, E. A.; Liao, J. H.; Pikramenou, Z.; Kanatzidis, M. G. *Chem. - Eur. J.* **1996**, *2*, 656.
- Li, H.; Malliakas, C. D.; Peters, J. A.; Liu, Z.; Im, J.; Jin, H.; Morris, C. D.; Zhao, L.-D.; Wessels, B. W.; Freeman, A. J.; Kanatzidis, M. G. *Chem. Mater.* **2013**, *25*, 2089.
- Chung, I.; Kanatzidis, M. G. *Chem. Mater.* **2014**, *26*, 849.
- Kyratsi, T.; Chrissafis, K.; Wachter, J.; Paraskevopoulos, K. M.; Kanatzidis, M. G. *Adv. Mater.* **2003**, *15*, 1428.
- Malliakas, C. D.; Chung, D. Y.; Claus, H.; Kanatzidis, M. G. *J. Am. Chem. Soc.* **2013**, *135*, 14540.
- Malliakas, C. D.; Chung, D. Y.; Claus, H.; Kanatzidis, M. G. *J. Am. Chem. Soc.* **2016**, *138*, 14694.
- Dhingra, S.; Kim, K.-W.; Kanatzidis, M. G. *MRS Proceedings*; 2011, p 204.

(24) Malliakas, C.; Billinge, S. J. L.; Kim, H. J.; Kanatzidis, M. G. *J. Am. Chem. Soc.* **2005**, *127*, 6510.

(25) Iordanidis, L.; Bilc, D.; Mahanti, S. D.; Kanatzidis, M. G. *J. Am. Chem. Soc.* **2003**, *125*, 13741.

(26) Chatterjee, A.; Biswas, K. *Angew. Chem., Int. Ed.* **2015**, *54*, 5623.

(27) Kanatzidis, M. G. *Acc. Chem. Res.* **2005**, *38*, 359.

(28) Mrotzek, A.; Kanatzidis, M. G. *Acc. Chem. Res.* **2003**, *36*, 111.

(29) Hoang, K.; Tomic, A.; Mahanti, S. D.; Kyratsi, T.; Chung, D. Y.; Tessmer, S. H.; Kanatzidis, M. G. *Phys. Rev. B: Condens. Matter Mater. Phys.* **2009**, *80*, 125112.

(30) Kim, J. H.; Chung, D. Y.; Kanatzidis, M. G. *Chem. Commun.* **2006**, *15*, 1628.

(31) Iordanidis, L.; Kanatzidis, M. G. *Inorg. Chem.* **2001**, *40*, 1878.

(32) Mrotzek, A.; Kanatzidis, M. G. *Acc. Chem. Res.* **2003**, *36*, 111.

(33) Mrotzek, A.; Chung, D. Y.; Ghelani, N.; Hogan, T.; Kanatzidis, M. G. *Chem. - Eur. J.* **2001**, *7*, 1915.

(34) Mrotzek, A.; Iordanidis, L.; Kanatzidis, M. G. *Chem. Commun.* **2001**, *17*, 1648.

(35) Hsu, K.-F.; Chung, D.-Y.; Lal, S.; Mrotzek, A.; Kyratsi, T.; Hogan, T.; Kanatzidis, M. G. *J. Am. Chem. Soc.* **2002**, *124*, 2410.

(36) Hsu, K.-F.; Lal, S.; Hogan, T.; Kanatzidis, M. G. *Chem. Commun.* **2002**, *13*, 1380.

(37) Kuznetsov, V.; Kuznetsova, L.; Rowe, D. *J. Appl. Phys.* **1999**, *85*, 3207.

(38) Ohta, M.; Chung, D. Y.; Kunii, M.; Kanatzidis, M. G. *J. Mater. Chem. A* **2014**, *2*, 20048.

(39) Kuznetsova, L.; Kuznetsov, V.; Rowe, D. *J. Phys. Chem. Solids* **2000**, *61*, 1269.

(40) Kuznetsov, V.; Kuznetsova, L.; Rowe, D. *J. Phys. D: Appl. Phys.* **2001**, *34*, 700.

(41) Shelimova, L.; Konstantinov, P.; Karpinskii, O.; Avilov, E.; Kretova, M.; Zemskov, V. *Inorg. Mater.* **2004**, *40*, 1146.

(42) Zemskov, V.; Shelimova, L.; Konstantinov, P.; Avilov, E.; Kretova, M.; Nikhezina, I. Y. *Inorg. Mater. Appl. Res.* **2012**, *3*, 61.

(43) Kuropatwa, B. A.; Kleinke, H. Z. *Anorg. Allg. Chem.* **2012**, *638*, 2640.

(44) Kuropatwa, B. A.; Assoud, A.; Kleinke, H. Z. *Anorg. Allg. Chem.* **2013**, *639*, 2411.

(45) Medlin, D. L.; Snyder, G. *JOM* **2013**, *65*, 390.

(46) Zhao, J.; Islam, S. M.; Kontsevoi, O. Y.; Tan, G.; Stoumpos, C. C.; Chen, H.; Li, R. K.; Kanatzidis, M. G. *J. Am. Chem. Soc.* **2017**, *139*, 6978.

(47) Tan, G.; Hao, S.; Zhao, J.; Wolverton, C.; Kanatzidis, M. G. *J. Am. Chem. Soc.* **2017**, *139*, 6467.

(48) Xia, Z.; Poepelmeier, K. R. *Acc. Chem. Res.* **2017**, *50*, 1222.

(49) Kikkawa, S. *Defect Diffus. Forum* **2001**, *191*, 1.

(50) Rouxel, J. *ACS Symp. Ser.* **1992**, *499*, 88.

(51) Delmas, C.; Braconnier, J. J.; Maazaz, A.; Hagenmuller, P. *Rev. Chim. Miner.* **1982**, *19*, 343.

(52) Hanko, J. A.; Sayettat, J.; Jobic, S.; Brec, R.; Kanatzidis, M. G. *Chem. Mater.* **1998**, *10*, 3040.

(53) X-AREA, X-R, and X-SHAPE; Cie & Stoe: Darmstadt, Germany, 1998.

(54) Sheldrick, G. *Acta Crystallogr., Sect. A: Found. Crystallogr.* **2008**, *64*, 112.

(55) (a) McCarthy, T. J.; Ngeyi, S. P.; Liao, J. H.; Degroot, D. C.; Hogan, T.; Kannewurf, C. R.; Kanatzidis, M. G. *Chem. Mater.* **1993**, *5*, 331. (b) Chondroudis, K.; McCarthy, T. J.; Kanatzidis, M. G. *Inorg. Chem.* **1996**, *35*, 840.

(56) de Boor, J.; Gupta, S.; Kolb, H.; Dasgupta, T.; Muller, E. J. *Mater. Chem. C* **2015**, *3*, 10467.

(57) Perdew, J. P.; Burke, K.; Ernzerhof, M. *Phys. Rev. Lett.* **1996**, *77*, 3865.

(58) Kresse, G.; Furthmüller, J. *Phys. Rev. B: Condens. Matter Mater. Phys.* **1996**, *54*, 11169.

(59) Zhao, L. D.; Lo, S. H.; Zhang, Y. S.; Sun, H.; Tan, G. J.; Uher, C.; Wolverton, C.; Dravid, V. P.; Kanatzidis, M. G. *Nature* **2014**, *508*, 373.

(60) Morelli, D.; Heremans, J.; Slack, G. *Phys. Rev. B: Condens. Matter Mater. Phys.* **2002**, *66*, 195304.

(61) Shannon, R. t. *Acta Crystallogr., Sect. A: Cryst. Phys., Diffraction, Theor. Gen. Crystallogr.* **1976**, *32*, 751.

(62) Kanatzidis, M. G.; McCarthy, T. J.; Tanzer, T. A.; Chen, L.-H.; Iordanidis, L.; Hogan, T.; Kannewurf, C. R.; Uher, C.; Chen, B. *Chem. Mater.* **1996**, *8*, 1465.

(63) Kim, J.-H.; Chung, D.-Y.; Kanatzidis, M. G. *Chem. Commun.* **2006**, *15*, 1628.

(64) Sassi, S.; Candolfi, C.; Ohorodniichuk, V.; Gendarme, C.; Masschelein, P.; Dauscher, A.; Lenoir, B. *J. Electron. Mater.* **2017**, *46*, 2790.

(65) Manos, M. J.; Ding, N.; Kanatzidis, M. G. *Proc. Natl. Acad. Sci. U. S. A.* **2008**, *105*, 3696.

(66) Mertz, J. L.; Fard, Z. H.; Malliakas, C. D.; Manos, M. J.; Kanatzidis, M. G. *Chem. Mater.* **2013**, *25*, 2116.

(67) Chung, D.-Y.; Iordanidis, L.; Rangan, K. K.; Brazis, P. W.; Kannewurf, C. R.; Kanatzidis, M. G. *Chem. Mater.* **1999**, *11*, 1352.

(68) Perdew, J. P.; Chevay, J. A.; Vosko, S. H.; Jackson, K. A.; Pederson, M. R.; Singh, D. J.; Fiolhais, C. *Phys. Rev. B: Condens. Matter Mater. Phys.* **1992**, *46*, 6671.

(69) Perdew, J. P.; Levy, M. *Phys. Rev. Lett.* **1983**, *51*, 1884.

(70) Manos, M. J.; Kanatzidis, M. G. *Chem. Sci.* **2016**, *7*, 4804.

(71) Chung, D.-Y.; Choi, K.-S.; Iordanidis, L.; Schindler, J. L.; Brazis, P. W.; Kannewurf, C. R.; Chen, B.; Hu, S.; Uher, C.; Kanatzidis, M. G. *Chem. Mater.* **1997**, *9*, 3060.

(72) Liu, H.; Shi, X.; Xu, F.; Zhang, L.; Zhang, W.; Chen, L.; Li, Q.; Uher, C.; Day, T.; Snyder, G. *J. Nat. Mater.* **2012**, *11*, 422.

(73) He, Y.; Day, T.; Zhang, T.; Liu, H.; Shi, X.; Chen, L.; Snyder, G. *J. Adv. Mater.* **2014**, *26*, 3974.

(74) Guin, S. N.; Chatterjee, A.; Negi, D. S.; Datta, R.; Biswas, K. *Energy Environ. Sci.* **2013**, *6*, 2603.

(75) Lin, H.; Tan, G.; Shen, J. N.; Hao, S.; Wu, L. M.; Calta, N.; Malliakas, C.; Wang, S.; Uher, C.; Wolverton, C. *Angew. Chem., Int. Ed.* **2016**, *55*, 11431.

(76) Li, H.; Peters, J. A.; Liu, Z.; Sebastian, M.; Malliakas, C. D.; Androulakis, J.; Zhao, L.; Chung, I.; Nguyen, S. L.; Johnsen, S.; Wessels, B. W.; Kanatzidis, M. G. *Cryst. Growth Des.* **2012**, *12*, 3250.

(77) Fulmer, J.; Lebedev, O. I.; Roddatis, V. V.; Kaseman, D. C.; Sen, S.; Dolyniuk, J. A.; Lee, K.; Olenov, A. V.; Kovnir, K. *J. Am. Chem. Soc.* **2013**, *135*, 12313.

(78) Shi, X.; Yang, J.; Salvador, J. R.; Chi, M.; Cho, J. Y.; Wang, H.; Bai, S.; Yang, J.; Zhang, W.; Chen, L. *J. Am. Chem. Soc.* **2011**, *133*, 7837.

(79) Nolas, G.; Morelli, D.; Tritt, T. M. *Annu. Rev. Mater. Sci.* **1999**, *29*, 89.

(80) Sales, B. C.; Chakoumakos, B. C.; Mandrus, D. *Phys. Rev. B: Condens. Matter Mater. Phys.* **2000**, *61*, 2475.

(81) Nolas, G. S.; Weakley, T. J. R.; Cohn, J. L.; Sharma, R. *Phys. Rev. B: Condens. Matter Mater. Phys.* **2000**, *61*, 3845.

(82) Hermann, R. P.; Jin, R.; Schweika, W.; Grandjean, F.; Mandrus, D.; Sales, B. C.; Long, G. *J. Phys. Rev. Lett.* **2003**, *90*, 135505.

(83) He, J.; Amsler, M.; Xia, Y.; Naghavi, S. S.; Hegde, V. I.; Hao, S.; Goedecker, S.; Ozoliņš, V.; Wolverton, C. *Phys. Rev. Lett.* **2016**, *117*, 046602.